Int J Adv Manuf Technol (2015) 77:1145–1154
DOI 10.1007/s00170-014-6449-4

ORIGINAL ARTICLE

Ultraprecision machining of diffraction optical elements on soft semiconductor crystal

Renato G. Jasinevicius · Paulo S. Pizani · Giuseppe A. Cirino

Received: 10 July 2014 / Accepted: 29 September 2014 / Published online: 6 November 2014

Abstract Diamond turning was used to generate microstructures on monocrystalline InSb. Different diffractive optical elements were machined (sinusoidal phase grating, continuous-phase Fresnel lens, and stepwise-phase Fresnel lens); the height of all features is in the micrometer range. The concept of transition pressure value was applied in order to demonstrate that it is possible to generate microstructures in rotational parts made of brittle semiconductors which can serve as the first-generation shim by employing electroforming process aiming for mass production of plastic optical parts. Results indicated that the aspect ratio suitable to sculpt microstructures by mechanical material removal processes applied to semiconductor crystals is directly related to its transition pressure value. Micro-Raman spectroscopy has been used to probe the phase transformation after machining and the recrystallization state after annealing.

Keywords Diamond turning · Indium antimonide · Single crystal · Diffractive optical elements · Phase transformation

R. G. Jasinevicius (✉)
Departamento de Engenharia Mecânica, Escola de Engenharia de São Carlos, Universidade de São Paulo, C.P. 359, São Carlos, São Paulo 13566-590, Brazil
e-mail: renatogj@sc.usp.br

P. S. Pizani
Departamento de Física, Universidade Federal de São Carlos, Caixa Postal 676, São Carlos, São Paulo 13565-905, Brazil

G. A. Cirino
Departamento de Engenharia Elétrica, Universidade Federal de São Carlos, São Carlos, São Paulo, Brazil

1 Introduction

The process of lithography applied to obtain micro-nanosized structures in semiconductors is normally referred as photolithography. The patterning method currently used consists of generating fine structures on the substrate by optical means, exposing using a mask as a reference in order to generate the pattern, chemical developing, and dry etching [1]. However, the application of mechanical material removal to generating micro- and or nanopatterns on semiconductor crystals can be considered a very challenging assignment. Literature has presented the possibility of nanomachining of semiconductors using a diamond tip to produce controlled features on GaAs with depths down to 10 Å as proposed by Goss et al. [2] and extended to other substrates such as GaSb, GaP, and InP by Grazulis et al. [3]. In this particular case, they have used a diamond tip to scan with a constant force along the substrate surface to produce the desired features with lateral resolutions as good as 100 Å. In addition, they have demonstrated that line profiles with cut depths ranging from 5 to 500 Å are feasible to obtain.

The possibility of applying diamond turning along with other lithography processes for the manufacturing of diffractive optical elements (DOEs) has shown to be successful [4, 5]. In both papers, they have shown the advantages of using diamond turning as a high-precision manufacturing process to produce 3D free-form optical surfaces with high-quality surface finish along with chemical etching processes. In the former case, they have machined a 3D microstructure with sub-micron features on the SU-8 photoresist and then the diffractive optical element (Fresnel lens) and a sine wave grating were transferred to the silicon substrate by precisely controlling the etch depth using a timed reactive ion etching technique. In the latter, they have produced molds for several types of liquid tunable microlenses and subsequently applied a

soft lithography process to replicate multiple lens structures from the fabricated mold. A different perspective to fabricate DOEs by using focused ion beam (FIB) milling to shape microtools with nanometric cutting edges with 25-nm cutting edges and complicated shapes to implement optical phase-modulation functions has been proposed [6]. These cutting tools with defined profiles are then used to fabricate micro-DOE with nanoscale finishes.

Furthermore, Yan and collaborators [7] have shown the application of diamond turning process to cut monocrystalline germanium using a V-type diamond tool and fabricate by a single-pass to cut Fresnel lens with form accuracy of 0.5 μm and average/rms roughness (R_q) ranging from 20 to 50 nm. The novelty in this paper is the cutting strategy used to generate a smooth and damage free surface in a typical brittle material.

The machining of semiconductor crystals is focused basically on silicon and germanium. The application of mechanical processes to sculpt semiconductor crystal substrate in the micro- and nanoscale may be considered a quest of meeting the cutting parameter dimensions with respect to the constrained volume of material that can be plastic deformed with suppression of the brittle response. This condition can be met whether the transition pressure value of each semiconductors crystal is taken into consideration. In 2000, Jasinevicius et al. [8] have reported results showing that the ductility presented by these materials may be related to its transition pressure value. According to the reported literature, the ductile response of normally brittle materials may be optimized based upon the transition pressure value: the smaller the transition pressure value of the semiconductor crystal, the larger the ductile response will be when it undergoes pressure and stress. The results showed that the maximum critical thickness of cut obtained for silicon and indium antimonide was 0.3 and 1.2 μm, respectively, using a round nose tool with 0.77 mm and −25° rake angle. This means that each semiconductor crystal may present a different volume of plastic deformation based upon its particular transition pressure value.

In metals' machining theory, for instance, the hardness of the material can be used to predict the ductile response of the pure metal and/or alloy during its machining. Nevertheless, in the case of semiconductors crystal, the hardness may not be considered a reliable parameter to use in order to evaluate the materials' ductile response when undergoing mechanical material removal processes [8]. Semiconductor crystals present a physical property called transition pressure value (Pt), which may be chosen as a more reliable parameter to predict its ductile response to mechanical material removal processes. This was first presented in a recent paper [9] in which three different semiconductor crystals were used to demonstrate this concept, to know: silicon (transition pressure value, Pt, with ~11.3<Pt<12.5 GPa, Vickers microhardness, $H_{Vickers}$, where ~11.3<$H_{Vickers}$<12.5 GPa), gallium arsenide (~16<Pt <18 GPa, $H_{Vickers}$~6<$H_{Vickers}$<6.5 GPa), and indium antimonide (Pt~2.3 GPa, $H_{Vickers}$~2.3 GPa) all with (001) crystallographic orientation. When these three materials were microindented with pyramidal Vickers indenters, they have shown a peculiar response: at first, it would be expected that the harder the material, the more brittle the response to mechanical contact will be. However, it was observed that under very small indentation loads (5 g), the GaAs sample presented a brittle response showing lateral cracks propagating at the vicinity of the indentation mark edge, whereas the Si and InSb sample presented a ductile imprint. This controversial behavior of GaAs has suggested that the brittle-to-ductile transition may be related to the transition pressure value, which is larger for this semiconductor crystal. In addition, the only probed difference was the size of the microindentation imprint, which follows the expected prediction, i.e., the harder the material, the smaller the volume plastically deformed. In the particular case of elemental semiconductor such as silicon, it was shown that the soft direction presented a ductile response during cyclic microindentation. Vickers test results brought about the confirmation that metastable phases are more easily generated in the [001] direction with lower number of cycles [10, 11], whereas this was only observed after 15 cycles in the soft direction [011]. Furthermore, the results also showed that the soft direction may present a ductile response during cyclic microindentation and conversely a brittle response to diamond machining. The authors [11] argued that the harder direction presented an inverse behavior: once the hardness value in the harder direction is similar to the transition pressure value of silicon, the ductile response was favored during machining and impaired during cyclic microindentation.

Based upon what have been exposed, this paper proposes that single-point diamond turning may well be considered a suitable method to be used as a mechanical microlithography manufacturing process to generating microstructure features on semiconductor crystals. Diamond turning tests were applied to single crystal InSb to generate three different microstructures: sinusoidal phase grating, continuous-phase Fresnel lens, and stepwise-phase Fresnel lens. Surface structural alteration was probed by micro-Raman spectroscopy.

2 Experimental details

Single-point diamond machining tests were carried out on a commercially available ultraprecision diamond turning machine, the Aspheric Surface Generator Rank Pneumo ASG 2500 with positioning resolution of 10 nm. The machining strategy used for all microstructures and the three different surface profiles proposed are shown in Fig. 1.

The machining tests were performed on samples in the form of squares (10×10 mm^2) cut from InSb (Wafer World,

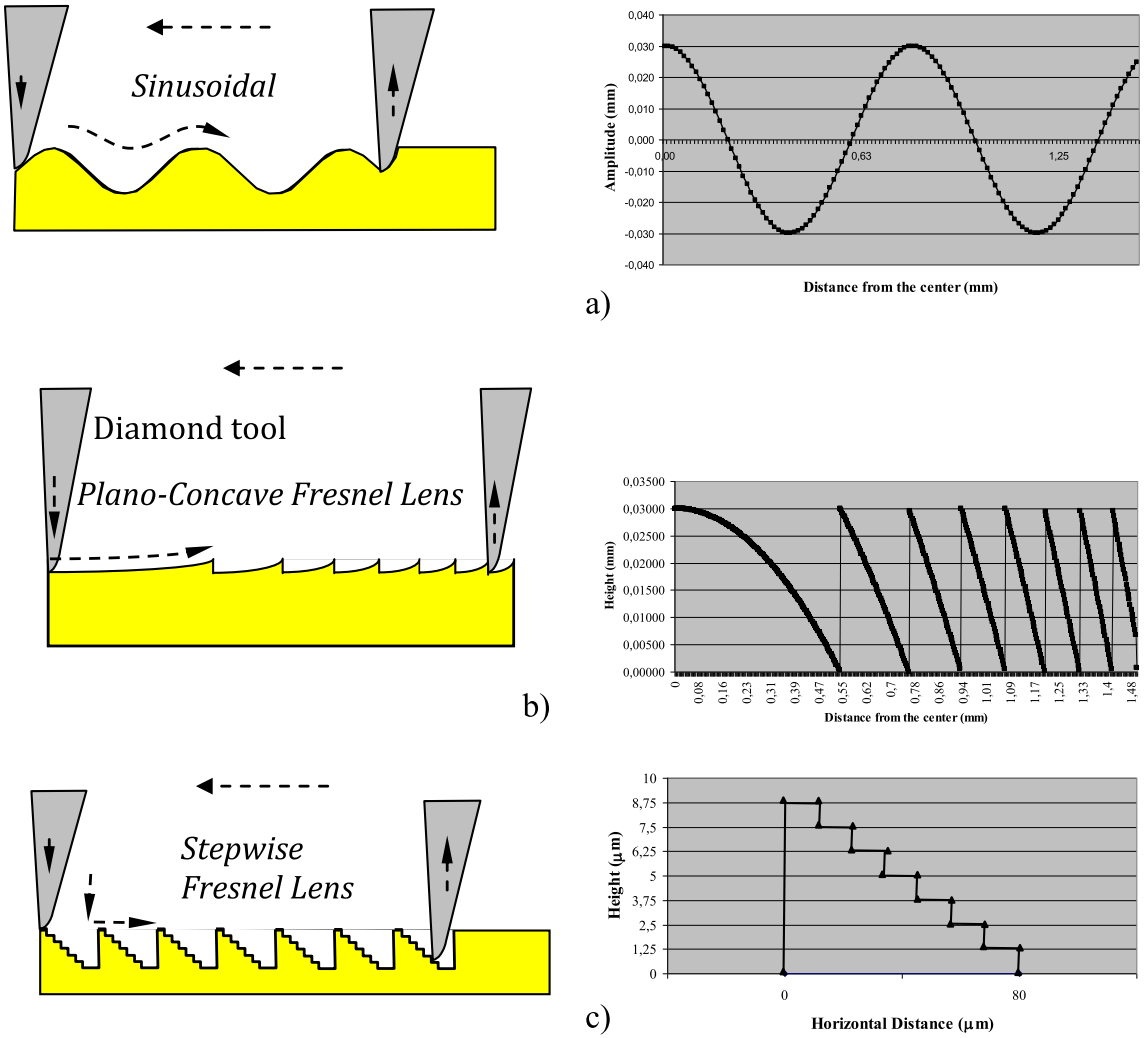

Fig. 1 Machining strategy applied to the fabrication mechanical lithography of microstructures in rotational parts and the graph plot for the points used in the NC program: **a** sinusoidal, **b** continuous-phase Fresnel lens, and **c** stepwise Fresnel lens

Inc.) wafers (001)±1° of 50.8 mm diameter, grade Prime, type N undoped, resistivity <0.6 E15 Ωcm and 450 μm thick with surface orientation. The cutting conditions for the three proposed structures are described in Table 1. The diamond cutting tool used to generate the microstructures has a special geometry with "half radius" made by Contour Fine Tooling (UK) and radius=0.047 mm, included angle=30°, rake angle=−25°, and primary clearance angle=10°.

A noncontact measurement system Wyko NT 1100 (Veeco Metrology Group) was used to measure the machined morphology and surface finish. The vertical-shifting interferometry (VSI) mode was chosen in this experiment. The vertical measurement range of this instrument is 0.1 nm to 1 mm, and the lateral spatial sampling 0.08 to 13.1 μm. The surface profiles were then plotted by Vision software from Veeco Instruments, Inc. Four measurements of the surface roughness were taken at every 90° quadrant, and average and standard deviation values were calculated.

The Raman measurements are performed using a T64000 Jobin-Yvon microspectrometer, using the 514-nm line of an argon ion laser. The laser power was kept below 1 mW, in order to avoid heating effects, an important care to be considered for analyzing highly disordered samples. The machined sample was heat treated by annealing in a microfurnace LINKAN TS-1500, and it was attached to the micro-Raman

Table 1 Cutting conditions used to generate the features into the InSb crystal surface

Microstructure	Fresnel	Sinusoidal	Stepwise Fresnel
Feed rate (μm/rev)	1		
Spindle speed (rpm)	1000		
Depth of cut (μm)	1	1	1.25 (each step)
Height (μm)	30	30	10 (total of 8)
Width (μm)	Variable	400	80

spectrometer in order to assess the recrystallization of the machined structures.

3 Results and discussion

In this section, the fabrication and characterization of the three proposed structures are detailed. Figure 2 presents schematically the tool paths of the cutting tool used to cut each one of the diffraction optical elements (DOEs) in the InSb crystal. For the three cases shown in Fig. 1, the crossfeed is from the center outwards; the tool moves in X and Z directions simultaneously to generate surface profiles.

3.1 Sinusoidal phase element

One- and two-dimensional sinusoidal phase gratings have been used in interferometric applications [12]. The sinusoidal phase profile has a diameter of 3 mm, 60 μm amplitude height, and 1.25 cycles/mm spatial frequency (Fig. 1a). The phase function for this element, which modulates an incident wavefront, is described by circular symmetry sinusoidal phase transmittance function [13].

Considering that a small region of this grating is illuminated, one can neglect its circular symmetry and assume a 1D structure. Additionally, if a unity-amplitude, normally incident plane wave illuminates the grating, and considering a far field observation plane, satisfying therefore the Fraunhofer approximation, the diffraction pattern generated by this sinusoidal grating will be given by the Fourier transform of its transmittance function (Eq. 1). The Fourier spectrum of such a phase structure comprises point-like diffraction orders of amplitude weighted by Bessel functions [12].

The 3D analysis plots of the machined sinusoidal element and its cross section surface profile are shown in Fig. 2a, b, respectively. The results showed good agreement with the designed profile. The surface roughness was also studied by using the optical profiler. Root mean square roughness (R_q) was obtained after machining evaluation of the surface. The average of the surface finish of the sample was obtained after three measurements. In this particular sample, the surface finish was measured in the downward portion and the upward. R_q=25.99±1.77 nm (upward portion) and 43.51±3.46 nm (downward portion) were estimated for the sinusoidal profile.

The observed discrepancy in the roughness values for the sinusoidal profile may be attributed to the tool path: the downward differs from the upward tool path cutting in terms of tool point portion interaction during surface roughness formation as it is shown in Fig. 3a–c. When the tool is moving downward, there is a considerable difference in surface roughness: the tool tip portion interacting with the machined surface will be the straight facet, as indicated in Fig. 3a, which is responsible for generating a rougher finish when compared to the upward movement interaction, which is primarily done by the round portion of the tool point the machined surface.

3.2 Continuous-phase Fresnel lens

The fabricated continuous-phase Fresnel lens has a diameter of 3 mm. It presents seven zones, with lens sag equal to 30 μm with variable zone width. The transition location for each zone occurs at $r_p^2=2.\lambda.p.f$ (where p=0, 1, 2, ….,7 is an integer number). Assuming a paraxial regime of operation, the phase function for this element, which modulates an incident wavefront, can be approximate to a quadratic phase distribution and is described by the following transmittance function [13].

$$tL(x,y) = 1.\exp[j\varphi L(x,y)] = \exp\left[-j\frac{k}{2f}\left(x^2+y^2\right)\right] \qquad k = \frac{2\pi}{\lambda} \tag{1}$$

where (x, y) is the 2D coordinates of the lens, f is its focal distance, k is the wave number, and λ is the operating wavelength. In order to implement a diffractive version of the lens, the phase function $\phi_L(x, y)$ is wrapped to an interval between 0 and an integer multiple of 2π, given by:

$$\phi N2\pi(x,y) = [\phi \mathrm{L}(x,y)]\mathrm{mod}N{\cdot}2\pi \tag{2}$$

where $\varphi_{N2\pi}$ (x, y) is the wrapped phase function and N is a positive integer ($0<\varphi_{N2\pi}<N.2\pi$). The surface relief profile must be implemented by generating a variation of the thickness $h(x, y)$ in a material with known refractive index at the operating wavelength, n. The thickness $h(x, y)$ is related to the phase profile $\varphi N2\pi$ (x, y) by

$$h(x,y) = \frac{\varphi_{N2\pi}(x,y)}{2\pi}\frac{\lambda}{(n-1)} \tag{3}$$

Figure 4a–d shows the results from the machining of the Fresnel lens. Figure 4a shows an overview of the machined Fresnel lens made by scanning electron microscope (SEM). The 3D image shown was built by stitching three regions measured (Fig. 4b). The cross section profile showed in Fig. 4c shows some disagreement in the amplitude height of the sample which is attributed to the stitching process used to join separated images. A surface finish image of the machined surface is shown in detail in Fig. 4d. Similarly to the wavefront sample, the cutting strategy used to generate the Fresnel finish follows the same route, but with a slight curvature at each Fresnel zone. The average value of the R_q roughness of the sample was 22±3.34 nm.

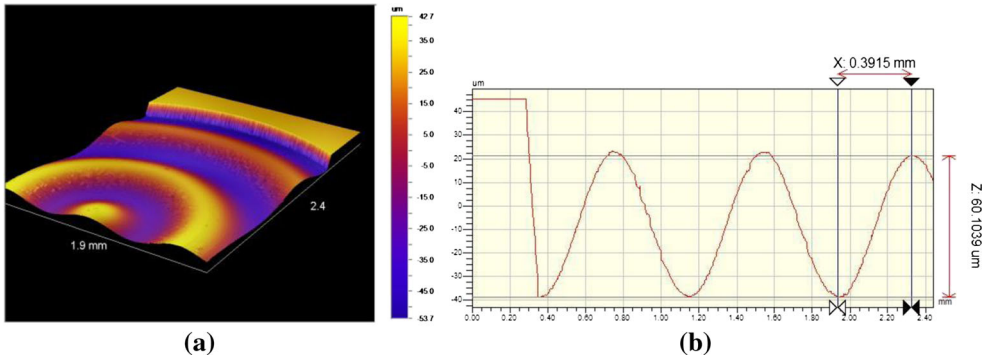

Fig. 2 Sinusoidal surface diamond turned **a** 3D images of the diamond turned sinusoidal surface and **b** cross section profile. (Color online)

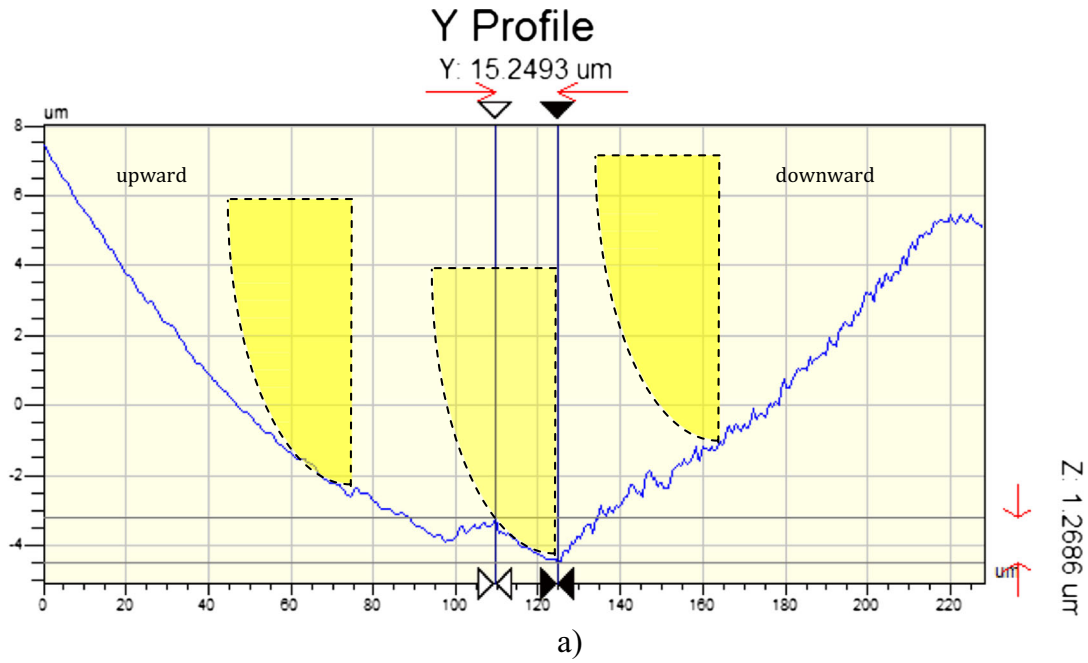

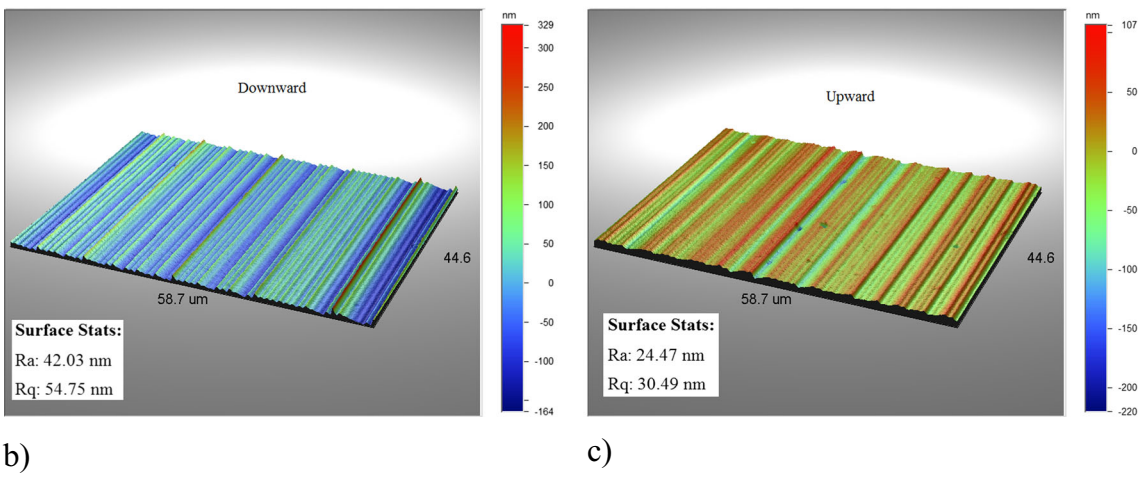

Fig. 3 Tool point portion interaction during machining of the sinusoidal profile. **a** Cross section analysis of the sinusoidal profile showing the schematic interaction of the tool and the surface generated-tool path model without considering tool radius/geometry compensation, **b** 3D image and surface finish values for the upward portion, and **c** 3D image and surface finish values for the upward portion; the surface roughness was estimated from an average of the results obtained from the steps surface

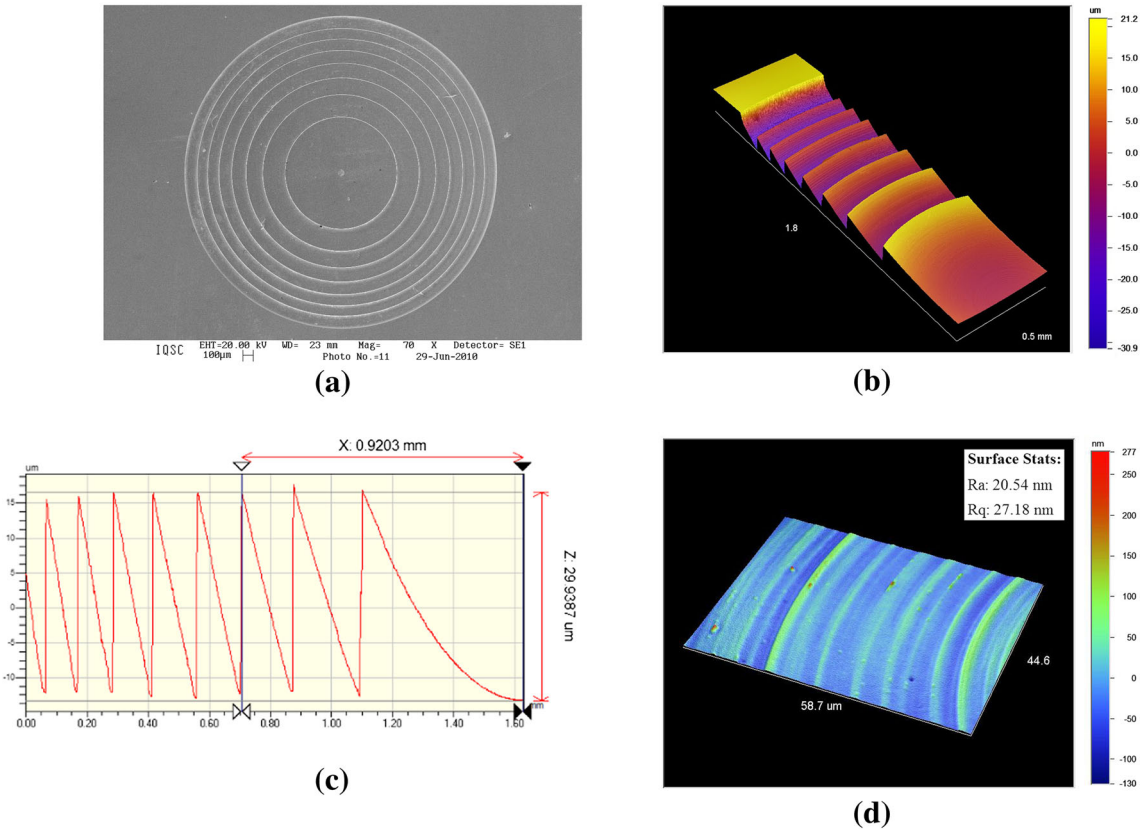

Fig. 4 Diamond turned continuous-phase Fresnel lens surface. **a** Scanning electron microscope image of the machined Fresnel lens, **b** 3D image of the diamond turned Fresnel zones, **c** cross section profile, and **d** 3D image showing the morphology of the surface finish obtained after machining. (Color online)

3.3 Stepwise-phase Fresnel lens

The stepwise-phase Fresnel lens has a diameter of 3 mm (Fig. 1c). It is composed of 16 zones including the center zone. Each zone has seven steps with 1.25 μm height and 10 μm width, which has an aspect ratio of 8:1. Fig. 1c shows a seven-zone continuous-phase Fresnel lens. The lens sag is 30 μm with variable zone width. The transition location for each zone occurs at $r_p^2 = 2.\lambda.p.f$ (where p=0, 1, 2,…,7 is an integer number).

The discretization of a continuous optical profile is known as binary optics due to the fact that these devices are fabricated by employing multiple binary lithographic masks. This approach generates diffractive structures with up to 2 N phase levels from N masks: each mask is able to double the number of phase levels [14, 15].

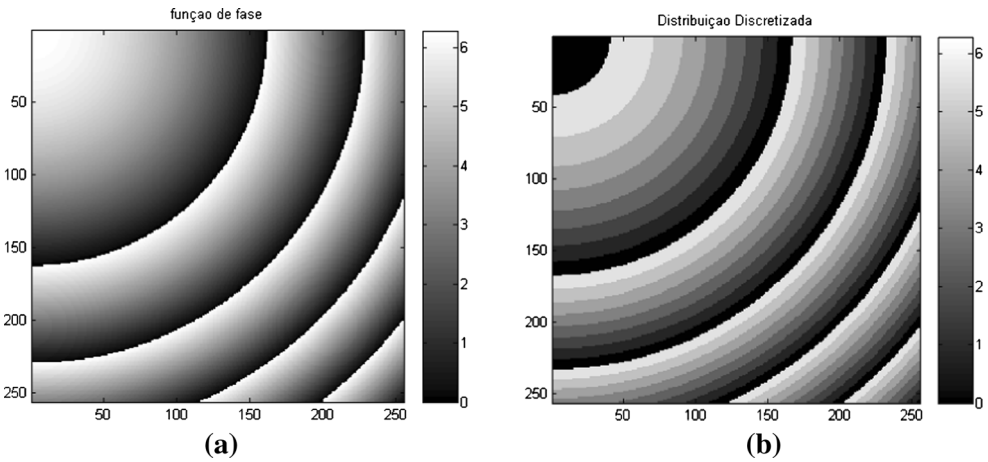

Fig. 5 Binarization process applied to a Fresnel lens **a** continuous-phase structure with 256 phase levels; **b** discretized phase distribution with eight phase levels. Only a quarter of the lens is shown

Table 2 Diffraction efficiency as a function of the number of phase levels (Eq. 6)

Number of phase levels, N	Diffraction efficiency, n
2	40.5
4	81.1
8	95.0
16	98.7

The binarization process of a continuous-phase structure is represented by the following operator:

$$\phi^{\mathrm{DISC}}{}_{N2\pi}(x,y) = \Delta\{\phi_{N2\pi}(x,y)\} \tag{4}$$

where $\phi^{\mathrm{DISC}}_{N2\pi}$ is resulting binarized phase distribution, $\phi_{N2\pi}$ is the continuous phase distribution described by Eq. 2, and $\Delta\{\}$ represents the binarization operator, defined by:

$$\phi^{\mathrm{DISC}}{}_{N2\pi}(x,y) = \Delta\{\phi_{N2\pi}(x,y)\}$$

$$= \begin{cases} 0 & \text{for } \left|\phi_{N2\pi}(x,y) - 1\pi/4\right| \le \left(\pi/8\right) \\ \pi/2 & \text{for } \left|\phi_{N2\pi}(x,y) - 2\pi/4\right| \le \left(\pi/8\right) \\ 3\pi/4 & \text{for } \left|\phi_{N2\pi}(x,y) - 3\pi/4\right| \le \left(\pi/8\right) \\ \pi & \text{for } \left|\phi_{N2\pi}(x,y) - 4\pi/4\right| \le \left(\pi/8\right) \\ 5\pi/4 & \text{for } \left|\phi_{N2\pi}(x,y) - 5\pi/4\right| \le \left(\pi/8\right) \\ 3\pi/2 & \text{for } \left|\phi_{N2\pi}(x,y) - 6\pi/4\right| \le \left(\pi/8\right) \\ 7\pi/4 & \text{for } \left|\phi_{N2\pi}(x,y) - 7\pi/4\right| \le \left(\pi/8\right) \end{cases} \tag{5}$$

Figure 5 illustrates the binarization process described by Eqs. 4 and 5 on a Fresnel lens. Figure 5a shows a continuous-phase structure with 256 phase levels, and Fig. 5b shows a discretized version of the phase distribution with 8 phase levels.

For this optical element, the transmittance function is a sampled version of Eqs. 4 and 5, where the phase and profile

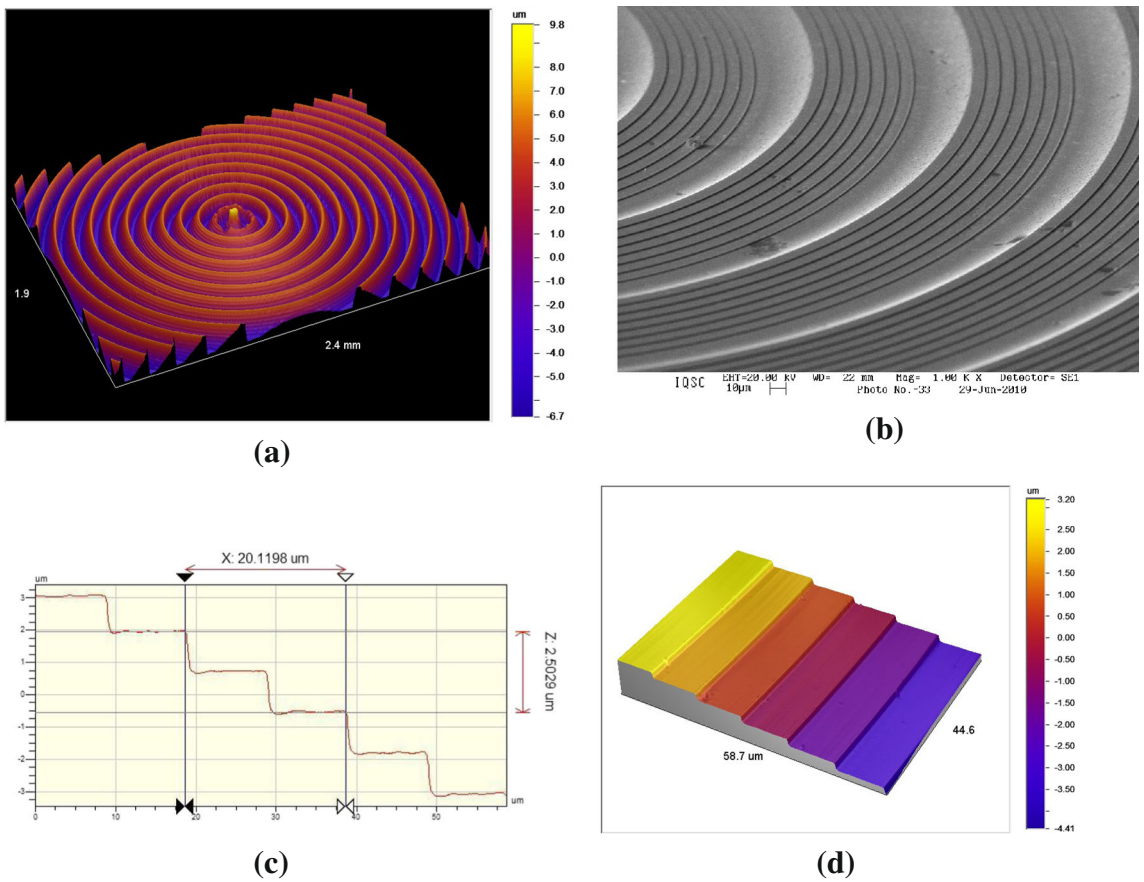

Fig. 6 Stepwise Fresnel lens surface diamond turned **a** 3D image of the diamond turned steps, **b** scanning electron microscope image of the machined steps, **c** cross section profile, and **d** 3D image showing the morphology of the square steps. (Color online)

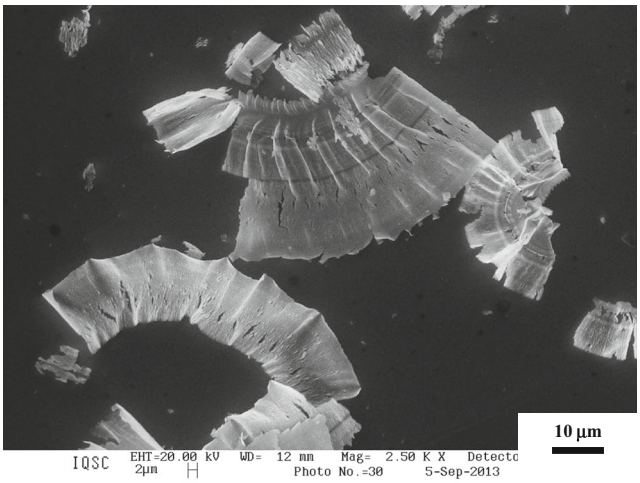

(a)

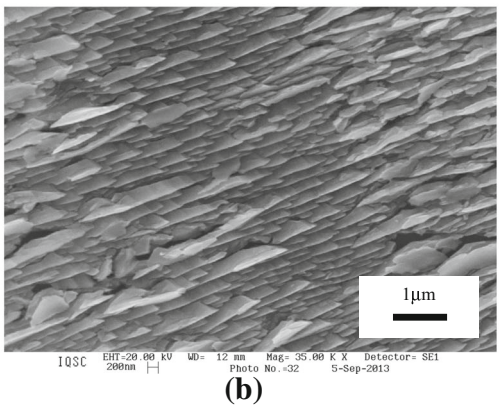

(b)

Fig. 7 **a** SEM image of the free surface InSb crystal chip found after machining in ductile mode and **b** detail view of the "lamellar" structure at high magnification. The lamellar structure in this case resembles very much "deformation bands"

height assume only a certain number of possible values. The impact of the limited number of phase levels can be observed in the diffraction efficiency, η, of the optical element. For linear gratings, the first-order diffraction efficiency is given by Swanson and Veldkamp [16]:

$$\eta = \left(\frac{\sin(\pi/M)}{(\pi/M)}\right)^2 \tag{6}$$

Equation 6 can be applied to estimate the efficiency of diffractive lenses. The lens structure is considered as local gratings with varying periods. In the central part of the lens, the grating periods are large and therefore the quantization of the phase profile is relatively simple and not critical. The grating period becomes smaller towards the rim, and the number of phase levels is limited by the fabrication process.

Table 2 shows the scaling of the efficiency η as a function of the number of phase levels. One can observe that 16 phase levels represent a good approximation of the continuous phase function, generated nearly the same diffraction efficiency [17].

The lens was measure by a Veeco NT1100 interferometer, as shown in Fig. 6a. A general view of the machined steps generated on the InSb sample may be seen in the scanning electron microscope (SEM) image shown in Fig. 6b. The image shows that the sample was cut mostly in the ductile mode. Figure 6c, d shows the cross section of the steps and the 3D image detail of the steps.

The surface finish results from the wavefront profile were obtained by measuring the surface finish of the flat portion of the step; three measurements were obtained, and the average was estimated. The surface roughness for the stepwise Fresnel was R_q=18±2.11 nm. The wavefront sample steps are generated by face cutting passes, and it is expected to have the best performance in terms of roughness once the cutting tool interaction is provided by a round nose tool. In this case, the roughness value is closely related to the feed and nose radius as shown in literature [18].

Although the microstructures fabricated in this study showed submicrometer scale resolution in the lateral direction, it is important to notice that there exist certain optical applications that would demand a higher accuracy. The machine tools commercially available nowadays work with positioning resolution in the picometer range. These improvements in machine tool precision along with fine sharped dedicated tools may well improve the results presented here. Ribbon-like chips found on the rake face of the tool after machining shows that the samples were machined mainly in the ductile mode (Fig. 7). In this case, only adhered material was found in the rake surface and no wear was detected in the cutting edge after the machining procedures.

Finally, it has to be considered that the machining of such semiconductor crystal may be applied for thermal imaging within the shortwave infrared (0.9–1.7 µm wavelength range), mediumwave infrared (3–5 µm), and longwave infrared (8–

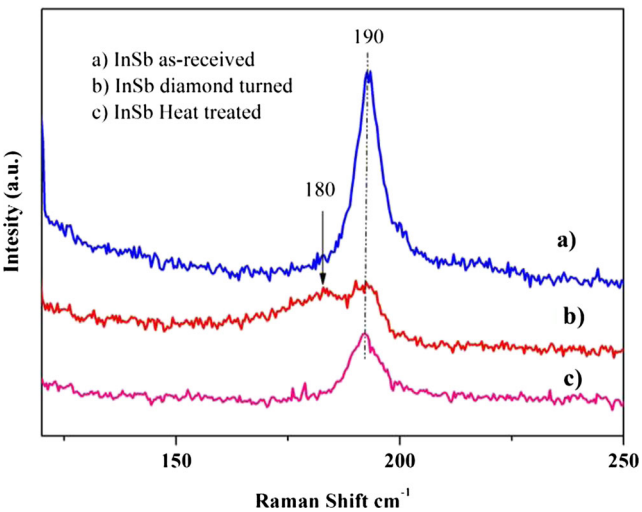

Fig. 8 Quasi-backscattering Raman spectrum of the diamond turned single-crystal InSb sample (*a*) before machining and (*b*) after machining in ductile mode

14 μm). In this case, even the largest roughness measured (Ra 43.51 nm) ranges from λ/68 to λ/115 of the focused wavelength and should contribute little to scatter and wave front distortion when considering the largest roughness considering the mediumwave infrared, for example.

3.4 Micro-Raman spectroscopy characterization of the machined sample

The machined surface structure and the crystalline phase recovery characterization were done by micro-Raman spectroscopy diagnostic. Spectrum a shown in Fig. 8 displays the quasi-backscattering Raman spectrum a for the InSb sample before machining, where it can be observed only the peak at ~190 cm^{-1}, due to the inelastic light scattering by the longitudinal optical phonon (LO), characteristic of the (001) oriented zinc blend structure. Spectrum b displayed in Fig. 8 shows the Raman spectrum after machining in the ductile mode. It can be observed an intensity reduction and a broadening of the LO peak, along with the merging of the peak at ~180 cm^{-1}, due to the inelastic light scattering by the transverse optical phonon (TO). These features are characteristic of the presence of a high short-range structural disorder into the vicinity of the surface, deriving from a phase transformation enabling the ductile response during machining. It was also observed that the cutting edge of the diamond tool, after machining, did not present any sign of wear. The good crystallinity of the InSb machined surface can be partially recovered by thermal treatments, as showed in Fig. 8c. It is worth to mention that the use of very high temperature may lead to chemical disorder into the machined surface due to the migration of Sb according to reported results [19].

These results demonstrated that structural disorder is present in ductile regime diamond turning of InSb crystal. This can be considered as indirect evidence that the plasticity, observed during machining of the microstructures, is related to a phase transformation in the cutting zone. Once InSb presents one of the lowest transition pressure values for semiconductor crystal, a high plasticity may be expected when mechanical material removal is applied to it and the ductile behavior of this material as the primary response mode to machining.

Based upon what have been shown, it is worth mentioning some advantages of using diamond turning as a mechanically lithography method:

(a) Rotational parts may be produced.
(b) Do not use hazardous chemical etchants to generate the pattern feature.
(c) Rapid process and environmentally friendly.
(d) Low tool wear for some semiconductors. No wear was detected in the cutting edge or the flank face of the diamond tool used in the tests. The wear mechanism that may take place during machining of this particular material has not been determined experimentally. Neither indium (In) nor antimony (Sb), and the compound semiconductor InSb as well, contain unpaired d-electron, which could induce chemical wear in diamond as thoroughly discussed by Paul and collaborators [20]. The wear of diamond tools during machining of semiconductor crystals still presents many gaps that demand more investigation.

4 Conclusions

The capability of fabricating small diffraction optical elements in single crystal semiconductor substrate by means of diamond turning was presented in this article. It is demonstrated that this method provides dimensional control and very low surface roughness for generating different types of diffraction optical surfaces that are normally obtained by conventional methods such as lithography and etching. It is shown that single-point diamond turning allows high-precision fabrication of features with variation in dimensions from micrometer range to submicrometer range. The application of diamond turning as an alternative method to generate microstructures in normally brittle materials is proposed as a mechanical lithography process with good results in terms of surface quality and dimensional accuracy. This is experimentally verified by the test results from the optical profiler and scanning electron microscope. To demonstrate the possibility of applying this fabrication method for optical applications, three different types of microstructures were generated. They are, namely, (1) sinusoidal, (b), continuous-phase Fresnel lens, and (c) stepwise-phase Fresnel lens. The application of the concept of phase transformation to meet the ductile response of brittle semiconductors shows the potential of using mechanical material removal process in order to generate fine structures on the substrate in micro- and nanoscale. Finally, it was demonstrated that the structural alteration generated by cutting tool material interactions may be recovered by means of a heat treatment process.

Acknowledgments This work was supported by the Brazilian research financing agency FAPESP—Fundação de Amparo a Pesquisa do Estado de São Paulo [Process no. 2008/536415 and Process no. 2007/56463-8].

References

1. Sinzinger S, Jahns J (2003) Microoptics. Willey-VCH, 437p
2. Goss SH, Grazulis L, Tomich DH, Eyink KG, Walck SD, Haas TW, Thomas DR, Lampert WV (1998) Mechanical lithography using a single point diamond machining. J Vac Sci Technol B 16(3):1439–1445

3. Grazulis L, Kelly DL, Walker DE Jr, Tomich DH, Eyink KG, Lampe WV (1999) Comparison of nanomachined III–V semiconductor substrates. J Vac Sci Technol B 17(4):1852–1855
4. Chen Y, Li L, Yi AY (2007) Fabrication of precision 3D microstructures by use of a combination of ultraprecision diamond turning and reactive ion etching process. J Micromech Microeng 17:883–890
5. Leung HM, Zhou G, Yu H, Chau FS, Kumar AS (2010) Diamond turning and soft lithography processes for liquid tunable lenses. J Micromech Microeng 20(2):025021
6. Xu ZW, Fang FZ, Zhang SJ, Zhang XD, Hu XT, Fu YQ, Li L (2010) Fabrication of micro DOE using micro tools shaped with focused ion beam. Opt Express 18(8):8025–8028
7. Yan J, Maekawa K, Tamaki J, Kuriyagawa T (2005) Micro grooving on single-crystal germanium for infrared Fresnel lenses. J Micromech Microeng 15:1925–1931
8. Jasinevicius RG, Pizani PS, Duduch JG (2000) Brittle to ductile transition dependence upon the transition pressure value of semiconductors in micromachining. J Mat Res 15(8):1688–1692
9. Jasinevicius RG, Pizani PS (2007) On the ductile response dependence upon phase transformation in diamond turning of semiconductors. Phys Status Solidi (b)244(1):261–265
10. Jasinevicius RG, Duduch JG, Pizani PS (2008) The influence of crystallographic orientation on the generation of multiple structural phases generation in silicon by cyclic microindentation. Mater Lett 62(6–7):812–815
11. Jasinevicius RG, Duduch JG, Montanaru L, Pizani PS (2012) Dependence of brittle-to-ductile transition on crystallographic direction in diamond turning of single-crystal silicon. Proc Inst Mech Eng B J Eng Manufact 226:445–458
12. Arellano NIT, Zurita GR, Garcia AM, Garcia DIS, Orduña, MGH, Experimental π phase-shifts observed in the Fourier spectra of phase gratings and applications in simultaneous PSI. In: Interferometry—research and applications in science and technology, Chapter 15, Intech Open Access, 2012 - *ISBN 978-953-51-0403-2*
13. Goodman JW (1996) Introduction to Fourier optics. 2nd Edition, chapter 4, p. 63
14. O'Shea DC, Suleski TJ, Kathman AD, Prather, DW (2004) Diffractive Optics: design, fabrication and test, Chapter 7, SPIE tutorial texts in optical engineering, Vol. TT62, SPIE Press, Belingham, Washington, pp. 133–148
15. Stern MB (1997) Binary optics fabrication. In: Micro-optics: elements, systems, and applications, H.P. Herzig, Ed. Taylor and Francis, London, pp. 53–85
16. Swanson GJ, Veldkamp WB (1989) Diffractive optical elements for use in infrared systems. Opt Eng 28:605–608
17. Hasman E, Davidson N, Friesem AA (1991) Efficient multilevel phase holograms for CO2 lasers. Opt Lett 16(6):423–425
18. Boothroyd G (1975) Fundamentals of metal machining and machine tools in *Chap. 5: Cutting fluids and surface roughness*, McGraw-Hill Book Co. pp.133–142.
19. Campos CEM, Pizani PS (2001) Studies of strain effects on As and Sb segregates immersed in annealed GaAs and GaSb by Raman spectroscopy J. Appl Phys 89(7):3631–3633
20. Paul E, Evans CJ, Mangamelli A, McGlauflin ML, Polvani RS (1996) Chemical aspects of tool wear in single point diamond turning. Precis Eng 18(1):4–19